Efficient Spectral Regulation in Ce:Lu3(Al,Cr)5O12 and Ce:Lu3(Al,Cr)5O12/Ce:Y3Al5O12 Transparent Ceramics With High Color Rendering Index for High-Power White LEDs/LDs

Tianyuan Zhou (529890234@qq.com)
Jiangsu Normal University
Chen Hou
Jiangsu Normal University
Le Zhang
Jiangsu Normal University
Yuelong Ma
Jiangsu University
Jian Kang
Jiangsu Normal University
Tao Li
Jiangsu Normal University
Rui Wang
Jiangsu Normal University
Jin Huang
Jiangsu Normal University
Junwei Li
Jiangsu Normal University
Zhongying Wang
Jiangsu Xiyi Advanced Materials Research Institute of Industrial Technology
Farida A Selim
Bowling Green State University
Ming Li
University of Nottingham
Hao Chen
Jiangsu Normal University

Research Article

Keywords: Ce,Cr:LuAG TC, spectral regulation, energy transfer, CRI, white LEDs/LDs

Posted Date: January 11th, 2021

DOI: https://doi.org/10.21203/rs.3.rs-142225/v1

Abstract

Realizing a high color rendering index (CRI) in Ce:LuAG transparent ceramics (TCs) with desired thermal stability is essential to their applications in white LEDs/LDs as color converters. In this study, based on the scheme of configuring the red component by Cr^{3+} doping, an efficient spectral regulation was realized in Ce,Cr:LuAG TCs. A unilateral shift could be observed in both PL and PLE spectra. By constructing TC-based white LED/LD devices in a remote excitation mode, luminescence properties of Ce,Cr:LuAG TCs were systematically investigated. The CRI values of Ce:LuAG TC based white LEDs could be increased by a magnitude of 46.2%. Particularly, by combining Ce,Cr:LuAG TCs with a 0.5 at.% Ce:YAG TC, a surprising CRI values of 88 and 85.5 were obtained in TC based white LEDs and LDs, respectively. Therefore, Ce,Cr:LuAG TC is a highly promising color convertor for high-power white LEDs/LDs applied in general lighting and displaying.

1. Introduction

White light emitting diodes (LEDs) and laser diodes (LDs) have considerable applications in general lighting, medical treatment and plant growth, etc., thanks to their advantages such as energy saving, environmentally friendly and high efficiency [1–3]. White LEDs/LDs are assembled by yellow conversion materials combining blue excitation sources, and the applied color conversion materials include phosphor powder, phosphor in glass, single crystal and transparent ceramic (TC) [4–6]. Among them, cerium doped yttrium aluminum garnet (Ce:YAG) TC has advantages of rich in doping ions, high ion doping concentration, desired mechanical property and high thermal conductivity [7, 8]. Also, Ce:YAG TC can overcome problems such as color deviation and easy aging that commonly occurred in the commercially available white LEDs/LDs, and has becoming a research focus currently.

However, lack of red component is the fundamental problem in Ce:YAG TC based white LEDs/LDs, resulting in their low color rendering index (CRI) and high correlated color temperature (CCT), which tremendously hinders their real applications [9]. Strategies such as co-doping red ions, regulating crystal field by substituting ions with similar ionic radius and coating red phosphors, were put forward by researchers to obtain high quality white light emissions in white LEDs/LDs [10–12]. Hu et al. altered the $5d^1$ energy level of Ce^{3+} ion via substituting Y^{3+} ions by Gd^{3+} ions in Ce:YAG TC, and the emission spectra of Ce^{3+} ion was red shifted by 16 nm [13]. Zhou et al. enhanced the emission properties of Ce:YAG TCs by co-doping moderate amount of Cr^{3+} ions, and found that the CRI values of the obtained TCs were increased by increasing Cr^{3+} ion doping concentration [14]. Jiang et al. observed a massive red shift from 533 nm to 598 nm in Ce:YAG TCs, by co-doping Mg^{2+} and Si^{4+} ions to substitute Al^{3+}-Al^{3+} pairs in YAG lattice [15]. Recently, our group obtained a broad emission within the orange-red region in Ce,(Pr,Mn):YAG TCs, through utilizing the “wide and narrow peak coupling effect” of Pr^{3+} and Mn^{2+} ions, and a high CRI value of 84.8 was realized [16]. Similar discoveries could be found elsewhere, such as Ce^{3+},Mn^{2+},Si^{4+}:YAG [17], Al_2O_3-Ce,Gd:YAG [18], Ce:$(Tb,Gd)_3Al_5O_{12}$ [19] and Ce:$Gd_3Al_4GaO_{12}$ [20], etc.. Additionally, it has been found that composite structure TCs are promising due to their high saturation threshold and excellent

thermal performance. Xu et al. found that the light homogeneity of Al_2O_3-YAG:Ce composite ceramic was far better than that of YAG:Ce single crystal, due to intense scattering by the phase/crystal boundaries [21]. A high thermal conductivity of 18.5 W/m·K and a remarkable thermal stability (only a 8% reduction at 200 ^oC) were realized in Al_2O_3-YAG:Ce composite ceramic. When irradiated under 445 nm blue laser, the ceramic shows no luminescence saturation even under a high power density of 50 W/mm^2 [22]. In general, regulating the transmission route of photon energy is significant to realize high quality luminescence in TC based white LED/LD devices.

Despite the red component could be increased by utilizing the above strategies, the thermal stability of TC was decreased simultaneously, owing to the relatively large ionic mismatch between doping ions and Y^{3+}/Al^{3+} ions in YAG lattice. On the contrary, the thermal stability of color convertor would be enhanced significantly, if Y^{3+} ion in YAG were completely substituted by Lu^{3+} ion with a smaller ionic radius to form LuAG. Xie et al. proved that the thermal stability of Ce:LuAG TC was far superior to that of Ce:YAG TC under the same Ce^{3+} concentration at 200 ^oC [23]. Additionally, only a 10% decreased PL intensity at 450 K compared to that of room temperature in Ce:LuAG TC was demonstrated by Wang et al [24]. Ce,Pr:LuAG TCs were fabricated by Shi et al. using the co-precipitated powders, and their luminescence properties at 550 nm were promoted effectively, thanks to the energy transfer between Pr^{3+} and Ce^{3+} ions [25]. In general, the luminescence property of TC based white LEDs/LDs could be further optimized, if applying LuAG TC as the color convertor.

In addition, current strategies with respect to promoting the luminescence properties of TCs mainly focus on adjusting the emission within the orange region (580–620 nm) [17, 26]. However, it should be noted that regulating the red region between 650 nm and 750 nm is significant to realize a standard white light emission. Therefore, it would be interesting and necessary to conduct a systematic research on regulating the red emission in Ce:LuAG TCs. Until now, however, few studies provide a clear insight on this issue. Considering the emission band of Cr^{3+} ion in garnet-structured material covers 650–800 nm region under 440 nm or 590 nm excitation, and a desired spectral regulation is expected, if doping Cr^{3+} ion into Ce:LuAG TC. Additionally, both the trajectory of photon energy and the energy transfer between Ce^{3+} and Cr^{3+} ions determine the red component of the emitted light of Ce,Cr:LuAG TC directly.

In this study, high quality Ce,Cr:LuAG TCs were fabricated by a solid state reaction sintering method under vacuum. The microstructural and spectral properties, as well as the energy transfer between Ce^{3+} and Cr^{3+} ions in LuAG TCs were investigated systematically. White LED/LD devices were also assembled by combining the as prepared TCs with blue LED chips/laser sources to evaluate their luminescence properties, with the purpose of providing a reference approach towards the spectral optimization within the red region in TCs. Finally, this work provides an effective strategy to advance the development and application of LuAG TC based light convertors for high power white LEDs/LDs.

2. Materials And Methods

2.1 Material preparation

High purity Lu_2O_3 (99.99%, Alfa Aesar, Ward Hill, America), α- Al_2O_3 (99.999%, Alfa Aesar, Ward Hill, America), CeO_2 (99.99%, Alfa Aesar, Ward Hill, America), Cr_2O_3 (99.9%, Alfa Aesar, Ward Hill, America) and Y_2O_3 (99.99%, Alfa Aesar, Ward Hill, America) powders were selected as the starting materials. They were weighted precisely using an analytical balance, and the detailed formula design of LuAG TCs was displayed in Table 1. Also, a 0.5 at.% Ce: YAG TC was fabricated to further optimize the luminescence performance of the constructed TC based LEDs/LDs. 0.5 wt.% tetraethyl orthosilicate (TEOS, 99.99%, Alfa Aesar, Ward Hill, America) was selected as the sintering additive to promote the densification of TCs during sintering.

Table 1
Ingredients of the Ce,Cr:LuAG TCs

Sample No.	Sample	Stoichiometry	Doping (at.%)	
			Ce	Cr
1	Ce0Cr01	$Lu_3(Al_{0.999}Cr_{0.001})_5O_{12}$	0	0.1
2	Ce01Cr0	$(Lu_{0.999}Ce_{0.001})Al_5O_{12}$	0.1	0
3	Ce01Cr01	$(Lu_{0.999}Ce_{0.001})_3(Al_{0.999}Cr_{0.001})_5O_{12}$	0.1	0.1
4	Ce01Cr02	$(Lu_{0.999}Ce_{0.001})_3(Al_{0.998}Cr_{0.002})_5O_{12}$	0.1	0.2
5	Ce01Cr03	$(Lu_{0.999}Ce_{0.001})_3(Al_{0.997}Cr_{0.003})_5O_{12}$	0.1	0.3
6	Ce01Cr04	$(Lu_{0.999}Ce_{0.001})_3(Al_{0.996}Cr_{0.004})_5O_{12}$	0.1	0.4
7	Ce01Cr05	$(Lu_{0.999}Ce_{0.001})_3(Al_{0.995}Cr_{0.005})_5O_{12}$	0.1	0.5
8	Ce01Cr06	$(Lu_{0.999}Ce_{0.001})_3(Al_{0.994}Cr_{0.006})_5O_{12}$	0.1	0.6

The powder mixtures were placed in high purity nylon ball milling jars with anhydrous ethyl alcohol as the milling agent, and planetary ball milled for 20 h under 150 rpm. The milled slurry was dried at 80 ^oC in an oven for 12 h in air, and then sieved though a 100-mesh screen. The sieved powders were uniaxially pressed into pellets with a diameter of 22 mm using a stainless-steel mold, and then placed into a high-pressure water tank and cold isostatic pressed (CIPed) at 200 MPa for 10 min to further increase their densities. The CIPed green bodies were calcined at 1000 ^oC for 3 h in a muffle furnace in air to remove residual volatile organic compounds. The sintering process was carried out at 1800 ^oC for 8 h under 10^{-3} Pa in a tungsten mesh heated vacuum furnace, and the applied heating rate was 2 ^oC/min. Finally, all the sintered TCs were annealed at 1400 ^oC for 25 h in air to remove the oxygen vacancies generated during vacuum sintering, and then grinded and mirror polished on both surfaces into 1 mm and 0.4 mm thickness for LuAG and YAG TCs, respectively.

2.2 Characterization

Phase compositions of the obtained TCs were identified by an X- ray diffraction machine (XRD; D8 Advance, Bruker, Karlsruhe, Germany) equipped with a copper target X- ray tube, and the selected scanning range (2θ) was 10-80^{o} with a step size of 0.01^{o}. In-line transmission spectra of the polished TCs were tested using a UV-VIS-NIR spectrophotometer (Lambda 950, Perkin Elmer, Waltham, MA, America) with a standard, dual light beam arrangement with adjustable slit width, and the applied scanning speed was 500 nm/min. Microstructural investigation of the sintered TCs was carried out by a scanning electron microscope (SEM; JSM- 6510, JEOL, Kariya, Japan). For the characterization of polished surfaces of TCs, they were thermal etched at 1450 ^{o}C for 2 h in air in a muffle furnace before SEM measurement. An energy dispersive X-ray spectrometer (EDS, Inca X-Max, Oxford Instruments, Oxford, England) connected with the SEM was utilized to recognize the element distribution of TCs. Photoluminescence (PL), photoluminescence excitation (PLE) and fluorescence decay spectra were detected by a spectrophotometer (FLS 980, Edinburgh Photonics, Edinburgh, England) with a scintillating xenon lamp. Chromaticity parameters of the prepared TCs were characterized using an integrating sphere (R98, Everfine, Hangzhou, China) assembled with 460 nm blue chips or a 450 nm laser source as the excitation sources, and the obtained spectroscopic data were processed by the system owned CAS-200 software. All the above measurements were carried out at room temperature.

3. Results And Discussion

Figure 1(a) shows the XRD patterns of LuAG TCs. All the diffraction peaks could be well indexed as the pure LuAG phase (PDF 97-018-2354), and there is no impurity phase (e.g., LuAM, LuAP, CeO_2 and Cr_2O_3) observed, indicating that the solid-state reaction between Lu_2O_3 and Al_2O_3 was completely finished during vacuum sintering. Increasing Cr^{3+} doping concentration hardly changed the phase composition of TCs, and there was no obvious peak shift observed from the main diffraction peaks of XRD patterns, owing to the low doping concentration of Cr^{3+} ion. Generally, Cr^{3+} ion (0.615 Å, CN = 6) would occupy the octahedral Al^{3+} site (0.53 Å, CN = 6), and Ce^{3+} ion (1.143 Å, CN = 8) would substitute the dodecahedral Lu^{3+} site (0.977 Å, CN = 8) in LuAG lattice [7, 27], owing to their similar ionic radius, as is shown in the schematic crystal structure sketch of Ce,Cr:LuAG TC in Fig. 1(b).

Appearances and in-line transmission spectra of the polished LuAG TCs are shown in Fig. 2. All the samples exhibited a transparent appearance, and the words behind them could be clearly recognized by the naked eyes. The color of the TC without Cr^{3+} doping (Ce01Cr0) was yellowish green, i.e., the intrinsic color of Ce^{3+} ion. With increasing Cr^{3+} doping concentration, the color of the TCs was changed from yellowish green to light green, indicating that the emission of the samples was tuned effectively by Cr^{3+} ion incorporation. From the transmission spectra it could be seen that moderate amounts of Ce^{3+} and Cr^{3+} doping hardly affected the transparency of TCs, and their transmittances at 800 nm were close to 70%. Increasing Cr^{3+} doping concentration deteriorated the transparency of TCs. The variation trend of

the transmittances at 800 nm and 400 nm of the prepared TCs could be found in Fig. 2(b). Two broad absorption bands centered at 340 nm and 445 nm were ascribed to the $4f$-$5d^1$ and $4f$-$5d^2$ transitions of Ce^{3+} ion, respectively [28, 29]. Besides the intrinsic absorption bands of Ce^{3+} ion, the absorption centered at 430 nm and 596 nm could be observed from all the Cr^{3+} ion doped samples, corresponding to the $^4A_2$-$^4T_1$ and $^4A_2$-$^4T_2$ transitions of Cr^{3+} ion, respectively [30].

Figure 3 shows the SEM micrographs of the sintered LuAG TCs. From the fracture surfaces of the samples (Fig. 3(a)-(h)) it could be seen that the fracture modes of all the samples were characterized by both intergranular and transgranular, and residual pores could be observed simultaneously, providing a quasi-densified microstructure. As can be seen from the polished surfaces of TCs (Fig. 3(a')-(h')), the amounts of residual pores were increased with increasing Cr^{3+} doping concentration, indicating that Cr_2O_3 affected the densification behavior of LuAG TCs during sintering. Also, feature of the residual pores was characterized by intergranular pores. Because the applied sintering temperature in this study was 1800 ^oC, which was lower than the ideal sintering temperature of LuAG TC, resulting in the intergranular pores in ceramic bulks. Generally, for the real application of TCs as color convertors for white LEDs/LDs, residual pores could act as light scattering centers to increase the light extraction rate [22, 31–33].

The variation trend of grain size as a function of Cr^{3+} doping concentration could be found in Fig. S1 of the Electronic Supplementary Information (ESI†), and it is obvious that the grain size of TCs was moderately increased with increasing Cr^{3+} doping concentration. However, the grain size of the fabricated TCs was only increased from 2.79 μm to 3.78 μm, owing to the relative low sintering temperature. Additionally, EDS mapping of the sintered Ce01Cr04 sample is shown in Fig. S2 in the ESI† to investigate its elemental distribution, and it could be found that all the adopted elements (Lu, Al, O, Ce and Cr) were distributed homogeneously inside ceramic bulk, indicating that both Ce^{3+} and Cr^{3+} ions were solid soluted into LuAG lattice without segregation [22, 31–33].

PL and PLE spectra of Ce0Cr01 sample is shown in Fig. 4(a). Recording at 687 nm, two broad absorption bands centered at 428 nm and 593 nm could be observed, originating from the $^4A_2$-$^4T_1$ and $^4A_2$-$^4T_2$ transitions of Cr^{3+} ion, respectively, leading to the characterized green color of Cr^{3+} doped LuAG TCs. By exciting Ce0Cr01 TC under 428 nm, an intensive broad emission band covered the orange-red and red color regions centered at 710 nm was obtained from the PL spectra. This emission was corresponded to the spin-allowed $^4T_2 \rightarrow {}^4A_2$ transition of Cr^{3+} ion. Simultaneously, a sharp R line (zero-phonon line) due to the spin-forbidden $^2E \rightarrow {}^4A_2$ transition could be detected at 690 nm, and a similar observation has been reported by researchers in Cr^{3+} doped garnet structured materials [34].

Figure 4(b) shows the normalized PLE spectra of Ce,Cr:LuAG TCs with different Cr^{3+} doping concentrations (λ_{em} = 523 nm). Two excitation bands centered at around 340 nm and 455 nm could be observed, corresponding to the $4f$-$5d^1$ and $4f$-$5d^2$ transitions of Ce^{3+} ion, respectively. Notably, a unilateral red shift phenomenon was observed from the left wing of the 410–500 nm band with increasing Cr^{3+}

doping concentration, whereas the right wing of this band was not influenced by Cr^{3+} doping. Combining with the PLE spectrum of Ce0Cr01 sample shown in Fig. 4(a), it could be deduced that a portion of the emitted photon of Ce^{3+} ion was absorbed by Cr^{3+} ion in Ce,Cr:LuAG TCs, resulting in a unilateral red shift of their PLE spectra [35]. Besides, it was speculated that the complicated local crystal environment around Ce^{3+} ions by doping Cr^{3+} ions into the [AlO_6] octahedron might be another reason that caused the unilateral red shift phenomenon [36].

Normalized PL spectra of Ce,Cr:LuAG TCs are displayed in Fig. 4(c). The characteristic broad emission band centered at 523 nm could be clearly resolved, corresponding to the 5*d*-4*f* transition of Ce^{3+} ion. The emission of Cr^{3+} ion could be detected simultaneously from all the Cr^{3+} doped samples. It could be clearly seen that the emission of Ce^{3+} ion overlapped with the absorption of Cr^{3+} ion. Therefore, Ce^{3+} ions in Ce,Cr:LuAG TC could not only acted as luminescence centers, but also as sensitizers proceeding the energy transfer from Ce^{3+} to Cr^{3+} ions, in which a portion of the photons emitted from Ce^{3+} ions could be absorbed by Cr^{3+} ions to realize red light emission. The energy transfer process from Ce^{3+} to Cr^{3+} ions could be processed through two means, i.e., radiative transition and non-radiative transition, and the detailed schematic diagram of the energy transfer process from Ce^{3+} to Cr^{3+} ions could be found in Fig. S3 (ESI†) [14]. The emission intensity of Cr^{3+} ions was increased with increasing Cr^{3+} doping concentration, and reached the maximum when the Cr^{3+} concentration was 0.5 at.% (Fig. 4(c)). Further increasing Cr^{3+} doping concentration decreased the emission intensity of TC, thanks to the concentration quenching effect. Besides, the right wing of the Ce^{3+} emission band was blue shifted as increasing Cr^{3+} concentration, whereas there was no obvious shift observed from the left wing of the band. This unilateral blue shift was owing to the increased absorption at around 593 nm that overlapped the PL spectra of Ce^{3+} ion as increasing Cr^{3+} ion doping concentration, which was similar to that of the observed unilateral red shift from the PLE spectra shown in Fig. 4(b). The detailed full width at half maximum (FWHM) values of both PL and PLE spectra of Ce^{3+} ion are presented in Fig. 4 (d), illustrating that Cr^{3+} ion doping could regulate the PL spectra of Ce^{3+} ion in Ce,Cr:LuAG TCs effectively.

In order to further validate the availability of the prepared TCs as fluorescent convertors, TC based white LED devices were constructed using the remote excitation mode. The operating power and the emitting wavelength of the blue LED chips were 20 W and 460 nm, respectively. Figure 5(a) shows the electroluminescent (EL) spectra of the TCs. It was evident that the sample without Ce^{3+} doping had a strong blue light emission, since the absorption ability of Cr^{3+} ion at 460 nm was far inferior than that of Ce^{3+} ion. Besides, the green component corresponding to the emission of Ce^{3+} ion was decreased with increasing Cr^{3+} doping concentration, thanks to the enhanced energy transfer from Ce^{3+} to Cr^{3+} ions. The variation trend of the chromaticity parameters is displayed in Fig. 5(b), and it could be found that with increasing Cr^{3+} doping concentration, the luminescence characteristic of white LEDs was changed from greenish to blueish.

Figure 5(c) shows the CRI values of Ce,Cr:LuAG TCs. It was obvious that the CRI values were increased with increasing Cr^{3+} doping concentration, and reached the maximum value of 75.7 for Ce01Cr03 TC. Further increasing Cr^{3+} doping concentration decreased the CRI values. The deteriorated CRI value was due to the proportional mismatch among red/green/blue light. Despite the optimized CRI value of 75.7 was not very ideal, it was much higher than that of the sample without Cr^{3+} doping, and the increment was as high as 46.2%.

The detailed variation trend of the red, green and blue light proportion is shown in Fig. 5(d). According to the system setting of CAS-200 software, the spectral bands of red/green/blue light were 600–780 nm, 500–600 nm and 380–500 nm, respectively, and the corresponding light proportion was obtained by calculating the ratio of the luminous flux of red/green/blue light to the total luminous flux collected by the integrating sphere. It could be seen from Fig. 5(d) that the red component was increased monotonously, whereas the greenish yellow light component was descended simultaneously. Because the blue light emitted from the chip was absorbed by the entire surface of TC under the remote excitation mode, and all the Cr^{3+} ions in TCs were not reached the saturation status, resulting in the continuous increased red light proportion in Ce,Cr:LuAG TC based white LEDs.

Fluorescence decay curves of Ce,Cr:LuAG TCs are plotted to further explore the energy transfer process from Ce^{3+} to Cr^{3+} ions under 460 nm excitation, as is shown in Fig. 6. The decay behavior of all the TCs could be fitted well by the single exponential decay function. From Fig. 6 it was obvious that with increasing Cr^{3+} doping concentration, lifetimes of Ce,Cr:LuAG TCs at 523 nm presented a monotonically decreasing trend, which was ranged from 55.52 ns (Ce01Cr00) to 33.47 ns (Ce01Cr04), illustrating an effective energy transfer from Ce^{3+} to Cr^{3+} ions.

The energy transfer efficiency was determined according to Eq. (1) [17, 37]:

$$\eta_T = 1-\tau/\tau_0 \quad (1)$$

where τ and τ_0 are the average lifetimes of the donor Ce^{3+} ions in the presence and without Cr^{3+} ions, respectively. With increasing Cr^{3+} doping concentration, the calculated η_T of Ce,Cr:LuAG TCs were 12.76%, 22.42%, 31.93% and 39.82%, respectively. It revealed that the energy transfer efficiency of TCs was promoted effectively by Cr^{3+} ion doping. The above results were in coincidence with that of the PL and EL spectra, demonstrating that Cr^{3+} ion doping is an effective approach to regulate the luminescence behavior of Ce:LuAG TC.

Judging from the EL spectra shown in Fig. 5, it was evident that the greenish yellow component of the single structure Ce,Cr:LuAG TC was inadequate. Therefore, scheme of combining Ce,Cr:LuAG TCs with a 0.5 at.% Ce:YAG TC was performed to further improve the luminescence performance of TC based white LEDs. Appearance and transmission spectra of the applied 0.5 at.% Ce:YAG TC could be found in Fig. S4 in the ESI†. Figure 7(a) presents the schematic sketch of TC based white LED device, in which Ce,Cr:LuAG TC was placed at the top of the LED device, and Ce:YAG TC was placed between Ce,Cr:LuAG TC and blue

LED chip. From the chromaticity parameters shown in Fig. 7(b) it could be seen that the color hue was regulated effectively by using the “ceramic combination strategy”, indicating the luminescence performance of white LEDs was significantly improved.

Figure 8 indicates the EL spectra and the corresponding CRI values of the white LEDs constructed with Ce:YAG and Ce,Cr:LuAG TCs as color convertors. It was noteworthy to see that the CRI values of the white LEDs were drastically promoted by using the “ceramic combination strategy”, which was in consistence with the optimized chromaticity parameters shown in Fig. 7(b). Surprisingly, by combining Ce:YAG TC with Ce01Cr04 TC, the obtained CRI value of white LEDs was as high as 88.0. Therefore, ratio of red/green/blue emission of white LEDs constructed with the combined TCs was more reasonable, compared with that of the white LEDs constructed with the single structure Ce,Cr:LuAG TCs. So it is obvious that the real sense emitting color of the assembled white LEDs was adjusted effectively by Cr^{3+} ion doping, as well as combining Ce,Cr:LuAG TCs with Ce:YAG TC, which is shown in the inserts of Fig. 8. Furthermore, the applied Ce^{3+} doping concentration in Ce,Cr:LuAG TCs could be further optimized, in order to obtain white light emission with a considerable CRI.

With respect to laser lighting test, the as-fabricated Ce,Cr:LuAG/Ce:YAG TCs were fixed on the aluminium alloy support frame with excellent heat dissipation performance to eliminate the possible thermal induced luminescence attenuation, and the appearance of the apparatus for LD measurement is shown in Fig. 9(a). It was composed of an integrating sphere and the constructed LD device. The detailed structure of the applied LD device could be found in our previous work [38]. Similar to the designation of the white LED device shown in Fig. 7, a 0.5 at.% Ce:YAG TC was also placed underneath the Ce,Cr:LuAG TCs to evaluate the luminescence performance of the constructed white LDs, and the applied excitation wavelength of the laser source was 450 nm. Also, the selected pump power of the laser source was 1 W, in order to avoid excessive local temperature that could deteriorate the luminescence performance of TCs during LD operation.

EL spectra of the combined Ce,Cr:LuAG/Ce:YAG TC based white LDs are shown in Fig. 9 (b). The sharp emission peak located at 450 nm was corresponded to the radiation of laser source with a narrow emission band. The emission bands of both Ce^{3+} and Cr^{3+} ions were clearly resolved when exciting TCs by a 450 nm blue laser source, and a distinct energy transfer from Ce^{3+} to Cr^{3+} ions could be observed simultaneously. Therefore, in addition to LED sources, the prepared LuAG TCs could also be excited effectively by blue laser sources with high energy density and tiny radiation area.

Figure 9(c) indicates the CRI values of the combined Ce,Cr:LuAG/Ce:YAG TCs as a function of Cr^{3+} doping concentration. Considering a portion of the transmitted blue light is highly directional compared to the emitted light from the TC. In this regard, a 1W blue laser was applied as the exciting source in this study, in order to avoid the side effect that could affect the CRI performance induced by the laser source. It was obvious that the obtained CRI values were regulated effectively by doping Cr^{3+} ions into Ce:LuAG TC. With increasing Cr^{3+} doping concentration, the yellow component of the emitted light was reduced, indicating a portion of the yellow light emitted from Ce^{3+} ions were absorbed by Cr^{3+} ions to increase the

red component of white LDs. It should be noted that the optimized CRI value was as high as 85.5, which was almost identical to that of the TC based white LEDs shown in Fig. 8.

However, from Fig. 9(d) it was found that the luminous flux of white LDs was moderately decreased from 257.3 lm to 218.5 lm with increasing Cr^{3+} doping concentration. Therefore, there existed a trade-off between CRI and luminous flux. The decreased luminous flux should be attributed to the energy loss originated from the increased yellow light absorption when increasing Cr^{3+} ion doping concentration. Nevertheless, from Fig. 9(c) it was noteworthy to see that the increment of CRI of white LDs was as high as 59.2%. Consequently, it was worthwhile to sacrifice a small fraction of luminous flux to realize a dramatic increased CRI in Ce,Cr:LuAG/Ce:YAG TC based white LDs. Finally, in addition to white LEDs, Ce,Cr:LuAG TC is also a considerable color convertor for the real applications of white LDs in the future.

4. Conclusions

This work illustrates that the luminescence performance of Ce:LuAG TC as a color convertor for white LEDs/LDs could be improved drastically by Cr^{3+} ion doping. The vacuum sintered Ce,Cr:LuAG TCs exhibited a pure phase microstructure with a homogeneous elemental distribution. Unilateral shift phenomenon was observed in both PLE and PL spectra of Ce,Cr:LuAG TCs. Notably, CRI of the prepared Ce:LuAG TC was increased by a magnitude of 46.2% by Cr^{3+} doping, owing to the optimized emitting light component. Besides, it was noteworthy that by combining Ce,Cr:LuAG TCs with a 0.5 at.% Ce:YAG TC, high CRI values of 88/85.5 for white LEDs/LDs could be obtained, thanks to the further optimized blue/green/red light proportion. In general, this study confirmed that Ce,Cr:LuAG TC is a potential light convertor for white LEDs/LDs, and its application prospect is foreseen in the future.

Declarations

Acknowledgement:

The authors acknowledge the generous financial support from the National Natural Science Foundation of China (61975070, 51902143, 61971207, 61775088), Priority Academic Program Development of Jiangsu Higher Education Institutions (PAPD), Key Research and Development Project of Jiangsu Province (BE2018062, BE2019033), Natural Science foundation of Jiangsu Province (BK20191467), Postgraduate Research & Practice Innovation Program of Jiangsu Province (KYCX18_2096, KYCX18_2097, KYCX18_2098, KYCX18_2099), International S&T Cooperation Program of Jiangsu Province (BZ2019063, BZ2020045, BZ2020030), and Special Project for Technology Innovation of Xuzhou City (KC19250, KC20201, KC20244). Special thanks to Xuzhou All-to Optoelectronics Co., Ltd. (Xuzhou, China) for the electro-luminescence characterization of the white LED/LD devices.

Compliance with ethical standards

Conflict of Interest: The authors declare that they have no conflict of interest.

References

1. Schubert EF, Kim JK, Solid-state light sources getting smart. *Science* 2005, **308:** 1274-1278.
2. Pimputkar S, Speck JS, DenBaars SP, *et al.* Prospects for LED lighting. *Nat Photonics* 2009, **3:** 180-182.
3. Liu X, Zhou H, Hu Z, *et al.* Transparent Ce:GdYAG ceramic color converters for high-brightness white LEDs and LDs. *Opt Mater* 2019, **88:** 97-102.
4. Nair GB, Swart HC, Dhoble SJ, A review on the advancements in phosphor-converted light emitting diodes (pc-LEDs): Phosphor synthesis, device fabrication and characterization. *Prog Mater Sci* 2020, **109:** 100622.
5. Ma X, Li X, Li J, *et al.* Pressureless glass crystallization of transparent yttrium aluminum garnet-based nanoceramics. *Nat Commun* 2018, **9:** 1175.
6. Xiang W, Zhong J, Zhao Y, *et al.* Growth and characterization of air annealing Mn-doped YAG:Ce single crystal for LED. *J Alloys Compd* 2012, **542:** 218-221.
7. Sun P, Hu P, Liu Y, *et al.* Broadband emissions from $Lu_2Mg_2Al_2Si_2O_{12}$:Ce^{3+} plate ceramic phosphors enable a high color-rendering index for laser-driven lighting. *J Mater Chem C* 2020, **8:** 1405-1412.
8. Meng Q, Wang X, Zhu Q, *et al.* The effects of Mg^{2+}/Si^{4+} co-substitution for Al^{3+} on sintering and photoluminescence of $(Gd,Lu)_3Al_5O_{12}$:Ce garnet ceramics. *J Eur Ceram Soc* 2020, **40:** 3262-3269.
9. Liu X, Qian X, Zheng P, *et al.* Preparation and optical properties of $MgAl_2O_4$-Ce:GdYAG composite ceramic phosphors for white LEDs. *J Eur Ceram Soc* 2019, **39:** 4965-4971.
10. Ao G, Tang Y, Yi X, *et al.* Red emission generation in Ce^{3+}/Mn^{2+} co-doping $Y_3Al_5O_{12}$ phosphor ceramics for warm white lighting emitting diodes. *J Alloys Compd* 2019, **798:** 695-699.
11. Hua H, Feng S, Ouyang Z, *et al.* YAGG:Ce transparent ceramics with high luminous efficiency for solid-state lighting application. *J Adv Ceram* 2019, **8:** 389-398.
12. Pricha I, Rossner W, Moos R, *et al.* Layered Ceramic Phosphors Based on $CaAlSiN_3$:Eu and YAG:Ce for White Light-Emitting Diodes. *J Am Ceram Soc* 2016, **99:** 211-217.
13. Hu S, Qin X, Zhou G, *et al.* Luminescence characteristics of the Ce^{3+}-doped garnets: the case of Gd-admixed $Y_3Al_5O_{12}$ transparent ceramics. *Opt Mater Express* 2015, **5:** 2902-2910.
14. Tang Y, Zhou S, Yi X, *et al.* The Cr-doping effect on white light emitting properties of Ce:YAG phosphor ceramics. *J Am Ceram Soc* 2017, **100:** 2590-2595.
15. Du Q, Feng S, Qin H, *et al.* Massive red-shifting of Ce^{3+} emission by Mg^{2+} and Si^{4+} doping of YAG:Ce transparent ceramic phosphors. *J Mater Chem C* 2018, **6:** 12200-12205.
16. Ma Y, Zhang L, Zhou T, *et al.* High recorded color rendering index in single Ce,(Pr,Mn):YAG transparent ceramics for high-power white LEDs/LDs. *J Mater Chem C* 2020, **8:** 4329-4337.
17. Wang B, Ling J, Zhou Y, *et al.* YAG: Ce^{3+},Mn^{2+} transparent ceramics prepared by gel-casting for warm white LEDs. *J Lumin* 2019, **213:** 421-426.

18. Liu X, Qian X, Hu Z, *et al.* Al_2O_3-Ce:GdYAG composite ceramic phosphors for high-power white light-emitting-diode applications. *J Eur Ceram Soc* 2019, **39:** 2149-2154.
19. Chen J, Tang Y, Yi X, *et al.* Fabrication of (Tb, Gd)$_3Al_5O_{12}$:Ce^{3+} phosphor ceramics for warm white light-emitting diodes application. *Opt Mater Express* 2019, **9:** 3333-3341.
20. Liu S, Sun P, Liu Y, *et al.* Warm White Light with a High Color-Rendering Index from a Single $Gd_3Al_4GaO_{12}$:Ce^{3+} Transparent Ceramic for High-Power LEDs and LDs. *ACS Appl Mater Interfaces* 2019, **11:** 2130-2139.
21. Xu J, Yang Y, Guo Z, *et al.* Comparative study of Al_2O_3-YAG:Ce composite ceramic and single crystal YAG:Ce phosphors for high-power laser lighting. *Ceram Int* 2020, **46:** 17923-17928.
22. Li S, Zhu Q, Tang D, *et al.* Al_2O_3–YAG:Ce composite phosphor ceramic: a thermally robust and efficient color converter for solid state laser lighting. *J Mater Chem C* 2016, **4:** 8648-8654.
23. Xu Y, Li S, Zheng P, *et al.* A search for extra-high brightness laser-driven color converters by investigating thermally-induced luminance saturation. *J Mater Chem C* 2019, **7:** 11449-11456.
24. Zhang Y, Hu S, Wang Z, *et al.* Pore-existing $Lu_3Al_5O_{12}$:Ce ceramic phosphor: An efficient green color converter for laser light source. *J Lumin* 2018, **197:** 331-334.
25. Jia-Yue XU, Ze-Qing SUN, De-Bao LIN, *et al.* Fabrication and Optical Properties of Ce, Pr Co-doped LuAG Transparent Ceramics. *J Inorg Mater* 2016, **31:** 1099.
26. Tang Y, Zhou S, Yi X, *et al.* The characterization of Ce/Pr-doped YAG phosphor ceramic for the white LEDs. *J Alloys Compd* 2018, **745:** 84-89.
27. Chen X, Hu Z, Feng Y, *et al.* Electronic band modification for faster and brighter Ce,Mg:$Lu_{3-x}Y_xAl_5O_{12}$ ceramic scintillators. *J Lumin* 2019, **214:** 116545.
28. Ma Y, Zhang L, Zhang L, *et al.* Fabrication and optical properties of divalent Cu^{2+} ions incorporated Ce:YAG transparent ceramics for white LEDs. *Ceram Int* 2019, **45:** 4817-4823.
29. Hu S, Lu C, Zhou G, *et al.* Transparent YAG:Ce ceramics for WLEDs with high CRI: Ce^{3+} concentration and sample thickness effects. *Ceram Int* 2016, **42:** 6935-6941.
30. Yi X, Zhou S, Chen C, *et al.* Fabrication of Ce:YAG, Ce,Cr:YAG and Ce:YAG/Ce,Cr:YAG dual-layered composite phosphor ceramics for the application of white LEDs. *Ceram Int* 2014, **40:** 7043-7047.
31. Tang Y, Zhou S, Chen C, *et al.* Composite phase ceramic phosphor of Al_2O_3-Ce:YAG for high efficiency light emitting. *Opt Express* 2015, **23:** 17923-17928.
32. Liu Z, Li S, Huang Y, *et al.* The effect of the porosity on the Al_2O_3-YAG:Ce phosphor ceramic: Microstructure, luminescent efficiency, and luminous stability in laser-driven lighting. *J Alloys Compd* 2019, **785:** 125-130.
33. Zhao H, Li Z, Zhang M, *et al.* High-performance Al_2O_3–YAG:Ce composite ceramic phosphors for miniaturization of high-brightness white light-emitting diodes. *Ceram Int* 2020, **46:** 653-662.
34. Xu T, Yuan L, Chen Y, *et al.* $Y_3Al_5O_{12}$:Ce^{3+} single crystal and red-emitting $Y_3Al_5O_{12}$:Cr^{3+} single crystal for high power W-LEDs. *Opt Mater* 2019, **91:** 30-34.

35. Feng S, Qin H, Wu G, *et al.* Spectrum regulation of YAG:Ce transparent ceramics with Pr, Cr doping for white light emitting diodes application. *J Eur Ceram Soc* 2017, **37:** 3403-3409.
36. Li S, Wang L, Zhu Q, *et al.* Crystal structure, tunable emission and applications of $Ca_{1-x}Al_{1-x}Si_{1+x}N_{3-x}O_x$:RE (x=0–0.22, RE=$Ce^{3+}$, Eu^{2+}) solid solution phosphors for white light-emitting diodes. *J Mater Chem C* 2016, **4:** 11219-11230.
37. Tong E, Song K, Deng Z, *et al.* Ionic occupation sites, luminescent spectra, energy transfer behaviors in $Y_3MgAl_3SiO_{12}$: Ce^{3+}, Mn^{2+} phosphors for warm white LED. *J Lumin* 2020, **217:** 116787.
38. Kang J, Zhang L, Li Y, *et al.* Luminescence declining behaviors in YAG:Ce transparent ceramics for high power laser lighting. *J Mater Chem C* 2019, **7:** 14357-14365.

Figures

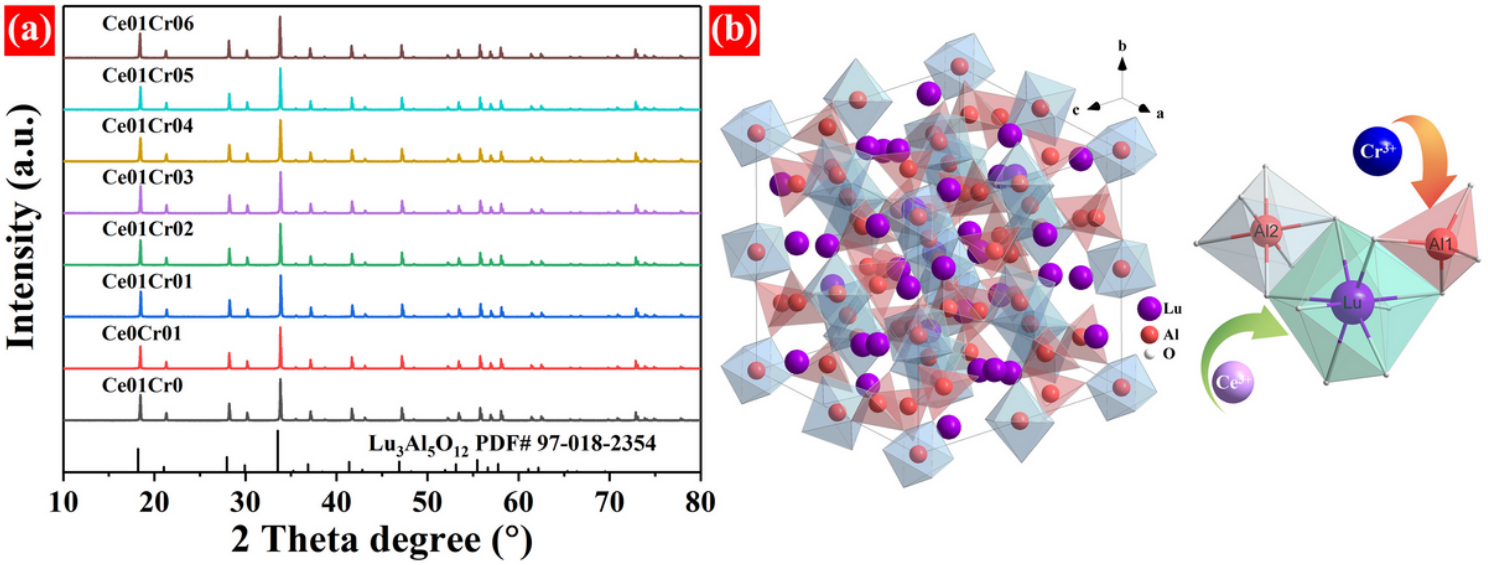

Figure 1

(a) XRD patterns and (b) schematic crystal structure sketch of Ce,Cr:LuAG TCs.

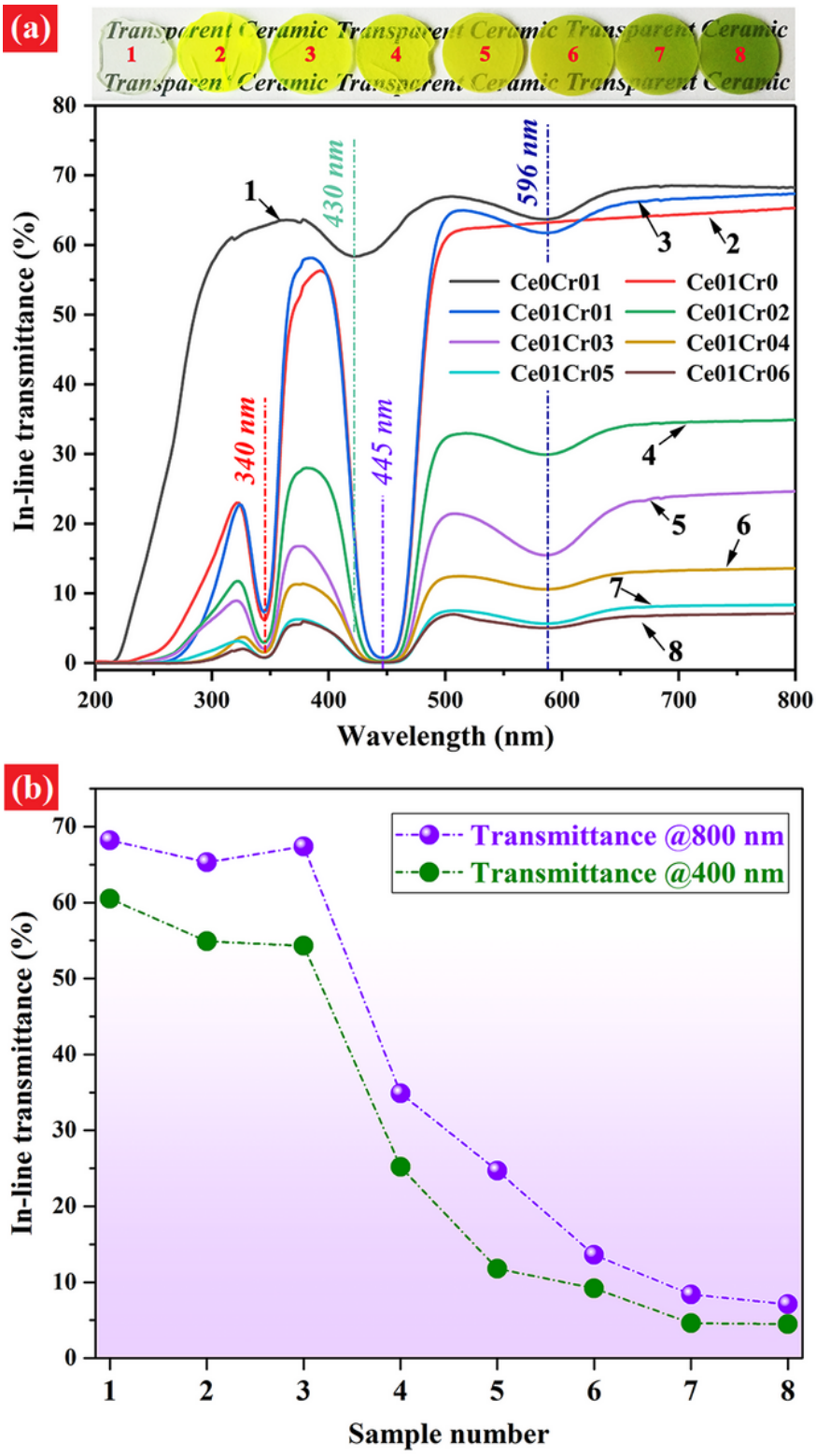

Figure 2

(a) Appearances and in-line transmission spectra of the Ce,Cr:LuAG TCs and (b) variation trend of the detailed transmittances at 800 nm and 400 nm of the prepared TCs.

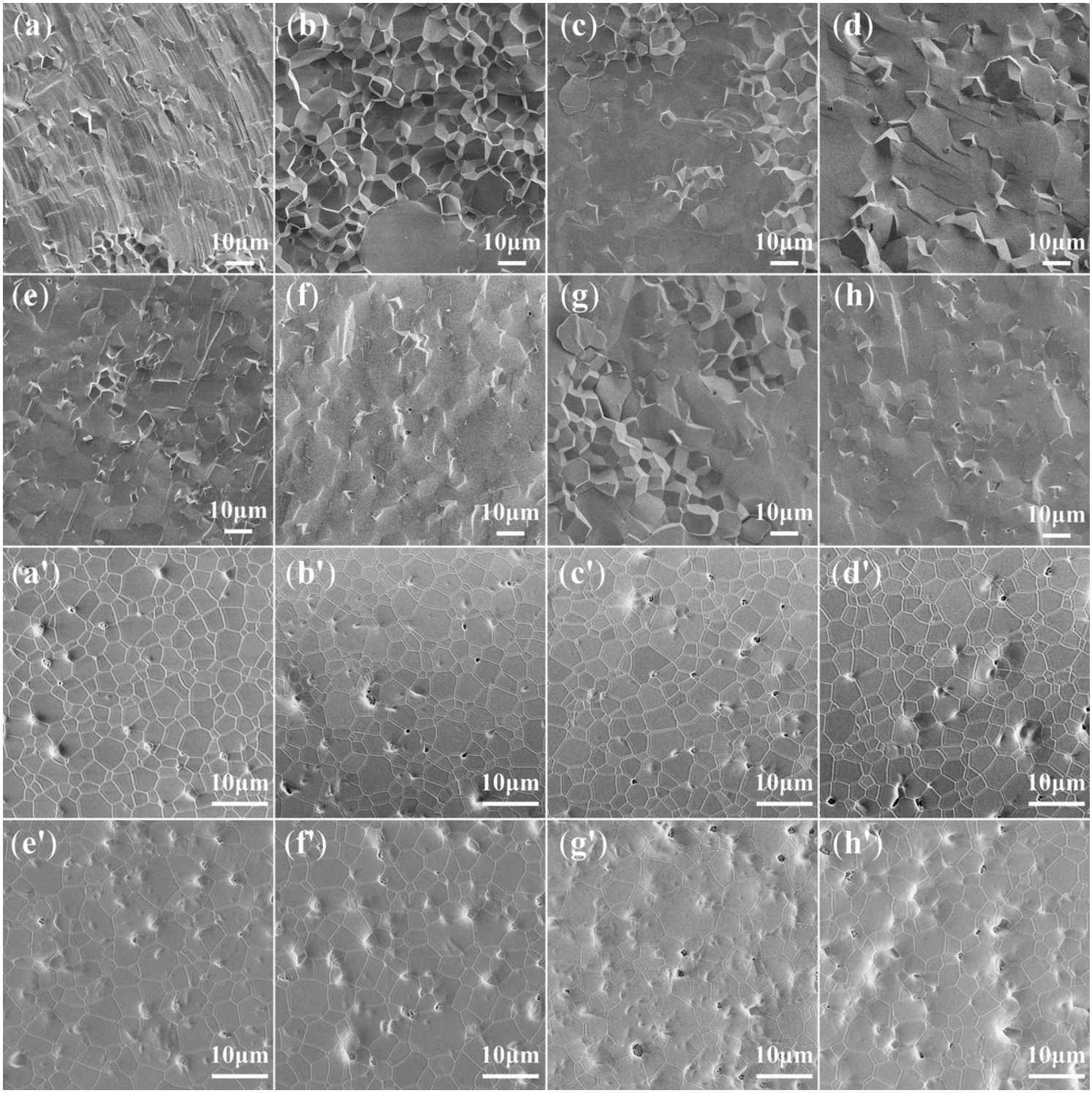

Figure 3

Fracture surfaces and polished surfaces of (a)-(a') Ce0Cr01, (b)-(b') Ce01Cr0, (c)-(c') Ce01Cr01, (d)-(d') Ce01Cr02, (e)-(e') Ce01Cr03, (f)-(f') Ce01Cr04, (g)-(g') Ce01Cr05, and (h)-(h') Ce01Cr06.

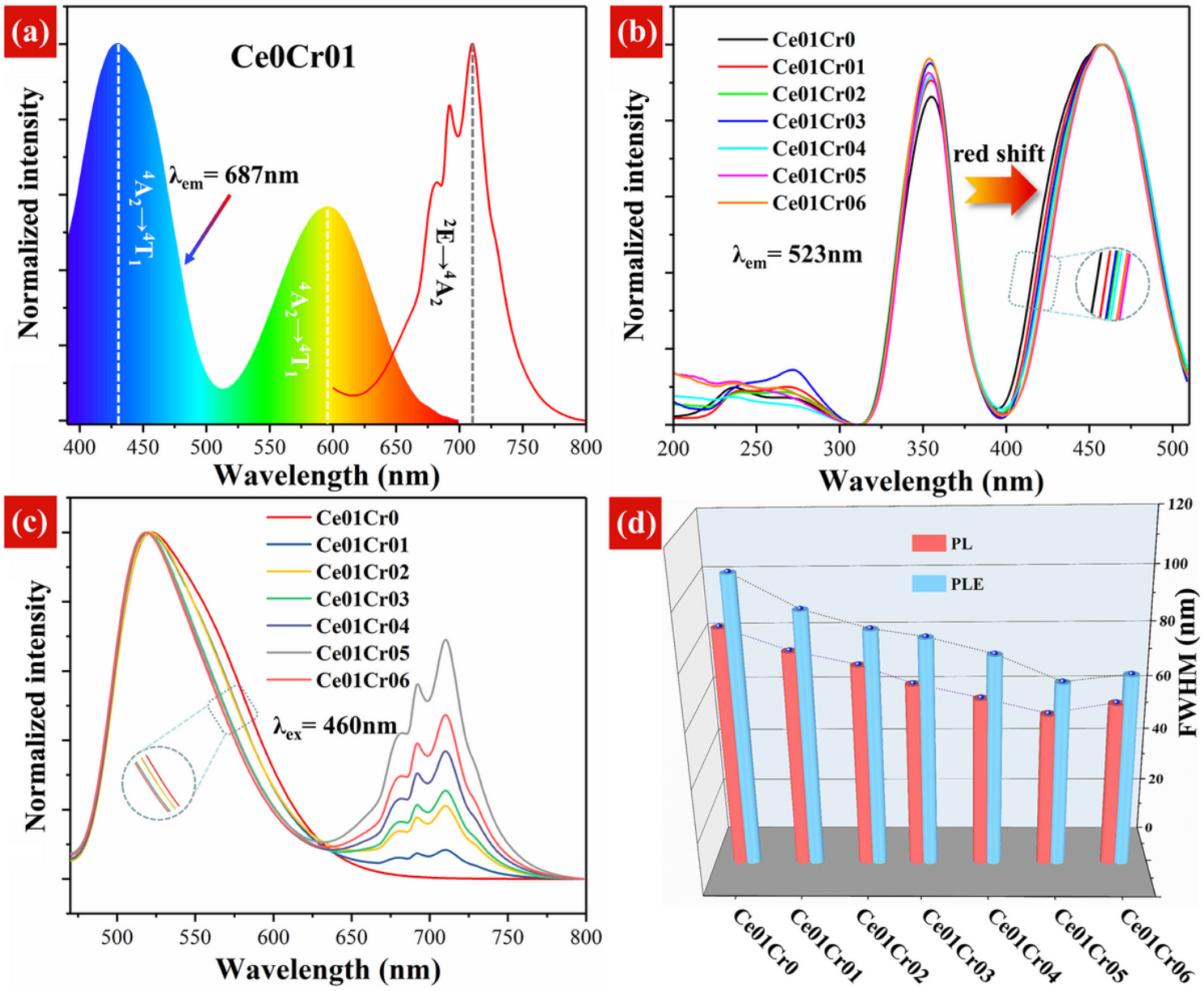

Figure 4

(a) PL and PLE spectra of Ce0Cr01 sample, (b) PLE and (c) PL spectra of Ce: LuAG and Ce,Cr: LuAG TCs, (d) FWHM values of PL and PLE spectra as a function of Cr3+ doping concentration.

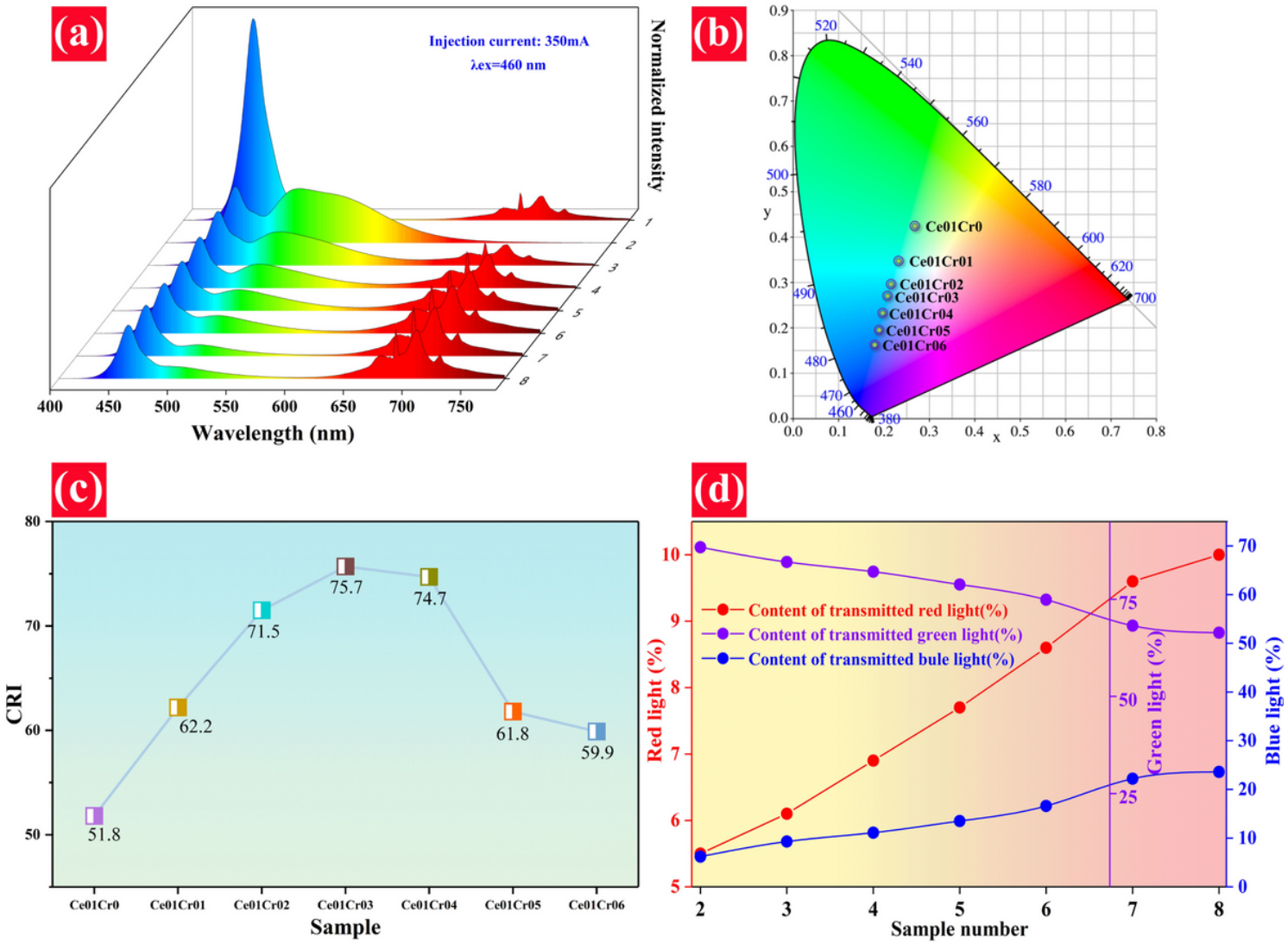

Figure 5

(a) EL spectra, (b) chromaticity parameters, (c) detailed CRI values and (d) variation trend of light proportion of the TC based white LEDs driven by 350 mA current.

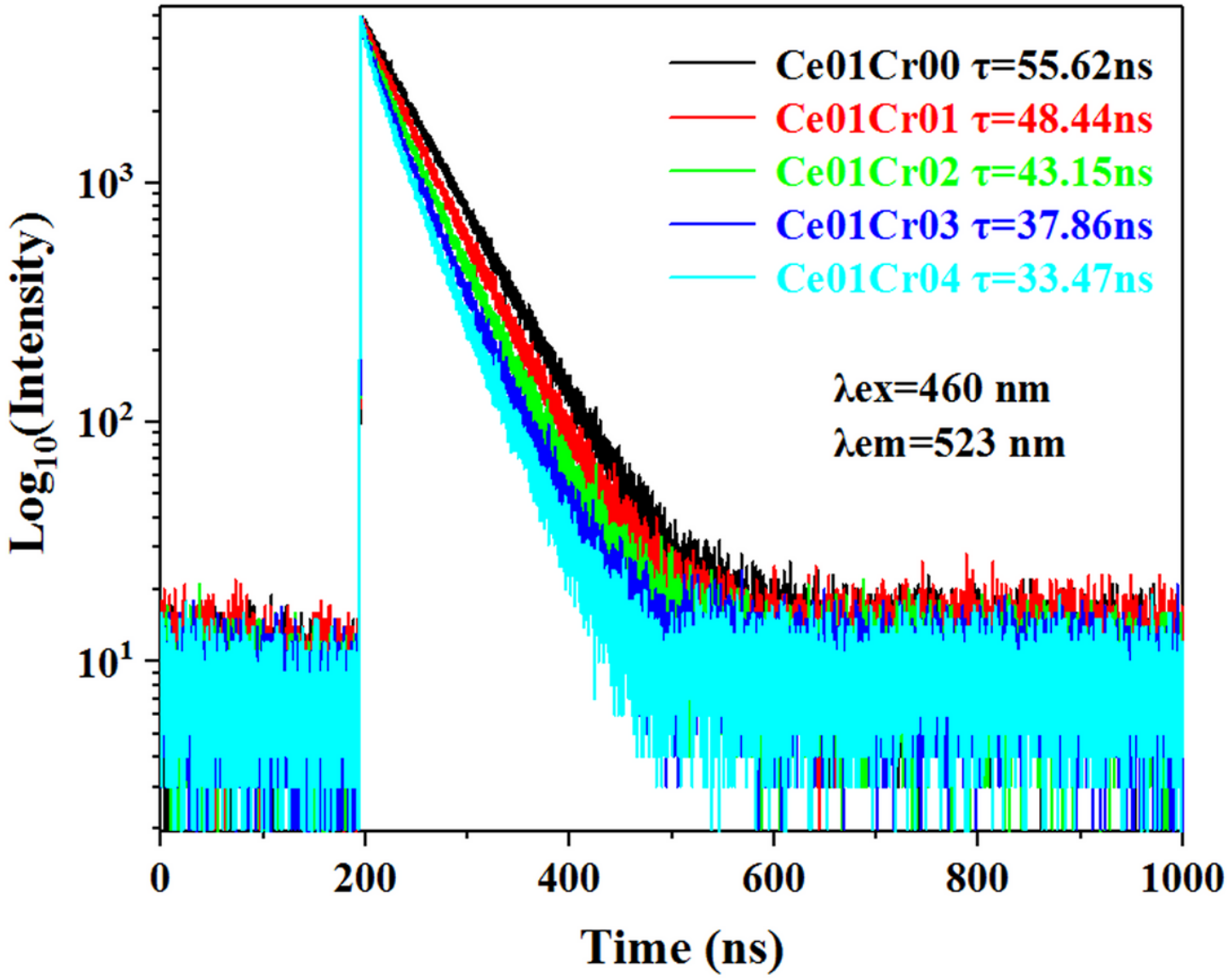

Figure 6

Fluorescence decay curves of Ce,Cr:LuAG TCs.

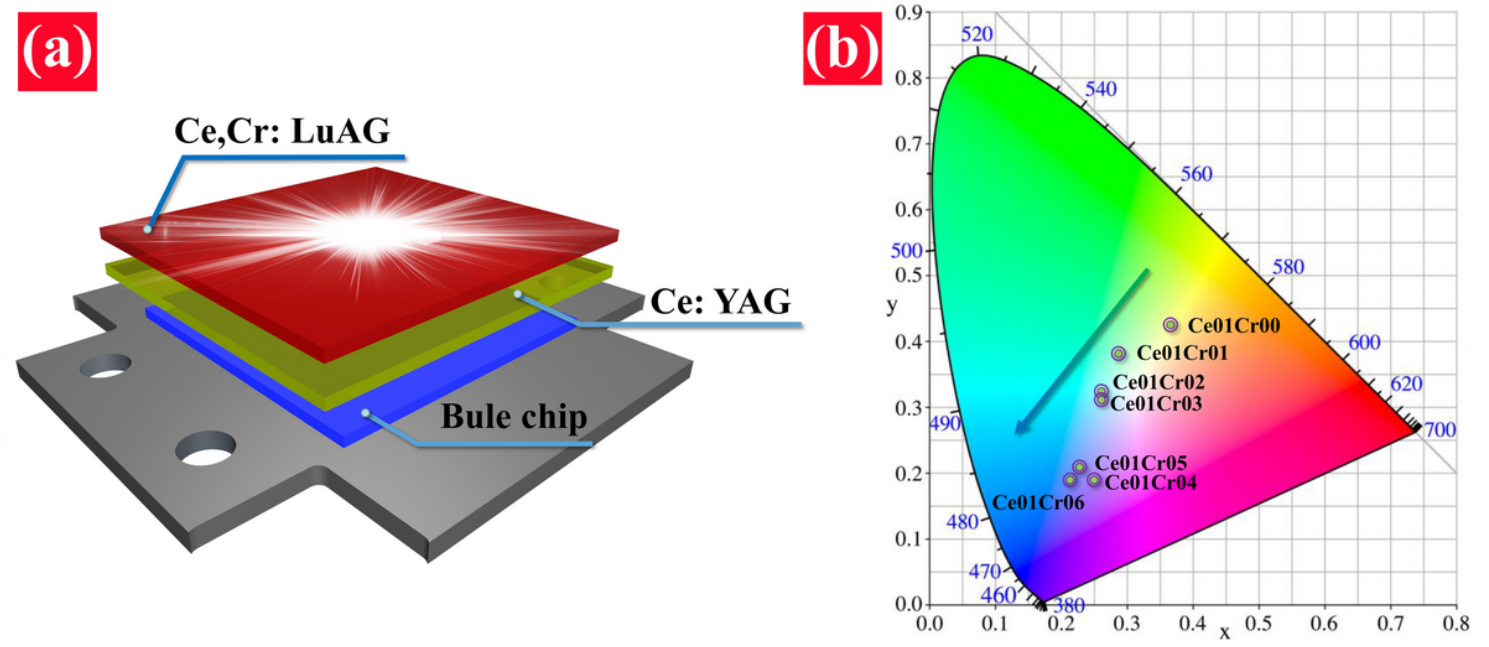

Figure 7

Schematic sketch of the white LED constructed with Ce:YAG and Ce,Cr:LuAG TCs and (b) the corresponding chromaticity parameters.

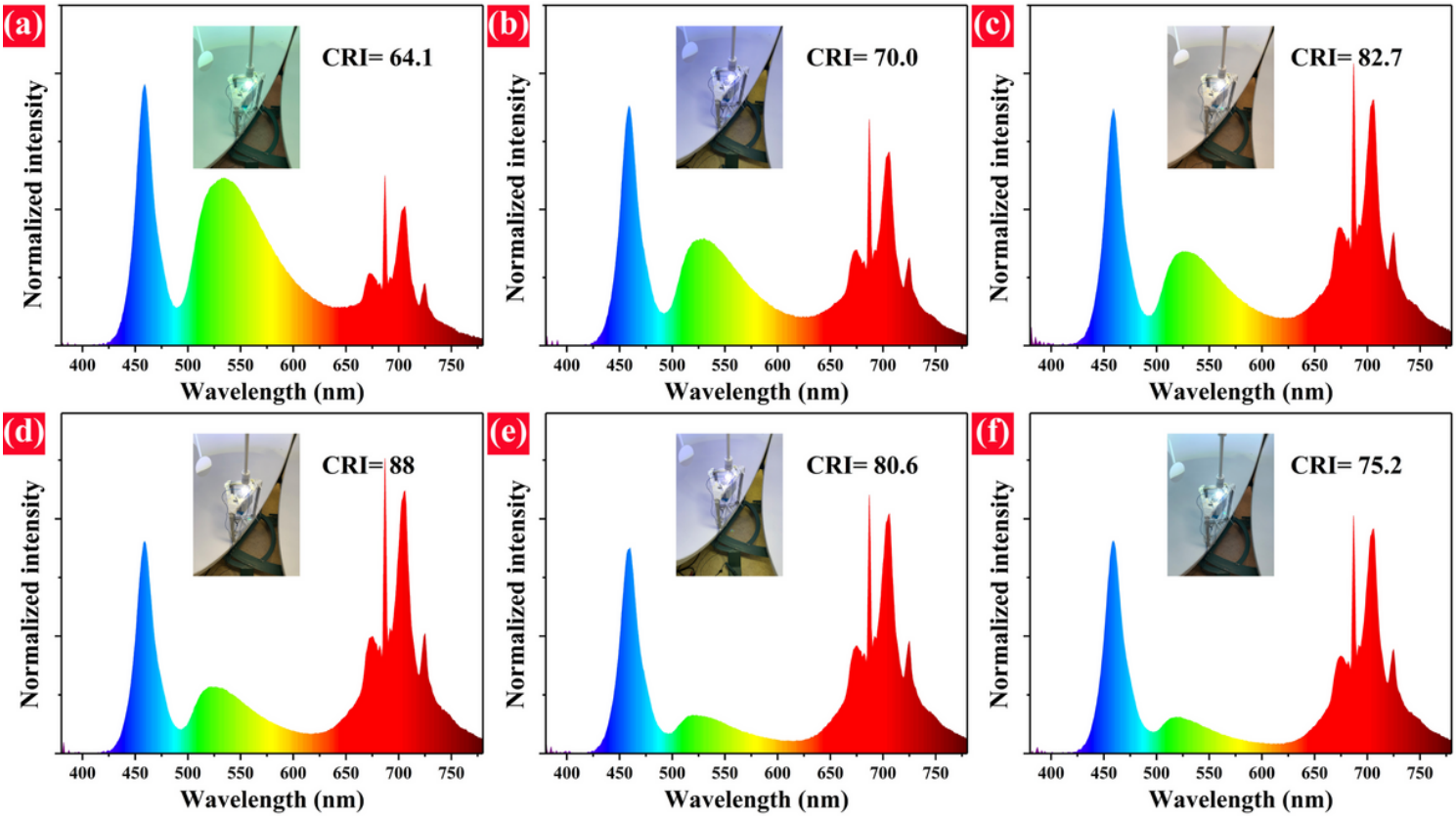

Figure 8

EL spectra and the corresponding CRI values of the white LED constructed with Ce:YAG combined with (a) Ce01Cr01, (b) Ce01Cr02, (c) Ce01Cr03, (d) Ce01Cr04, (e) Ce01Cr05 and (f) Ce01Cr06 TCs and their real sense visual renderings during LED operation (insert).

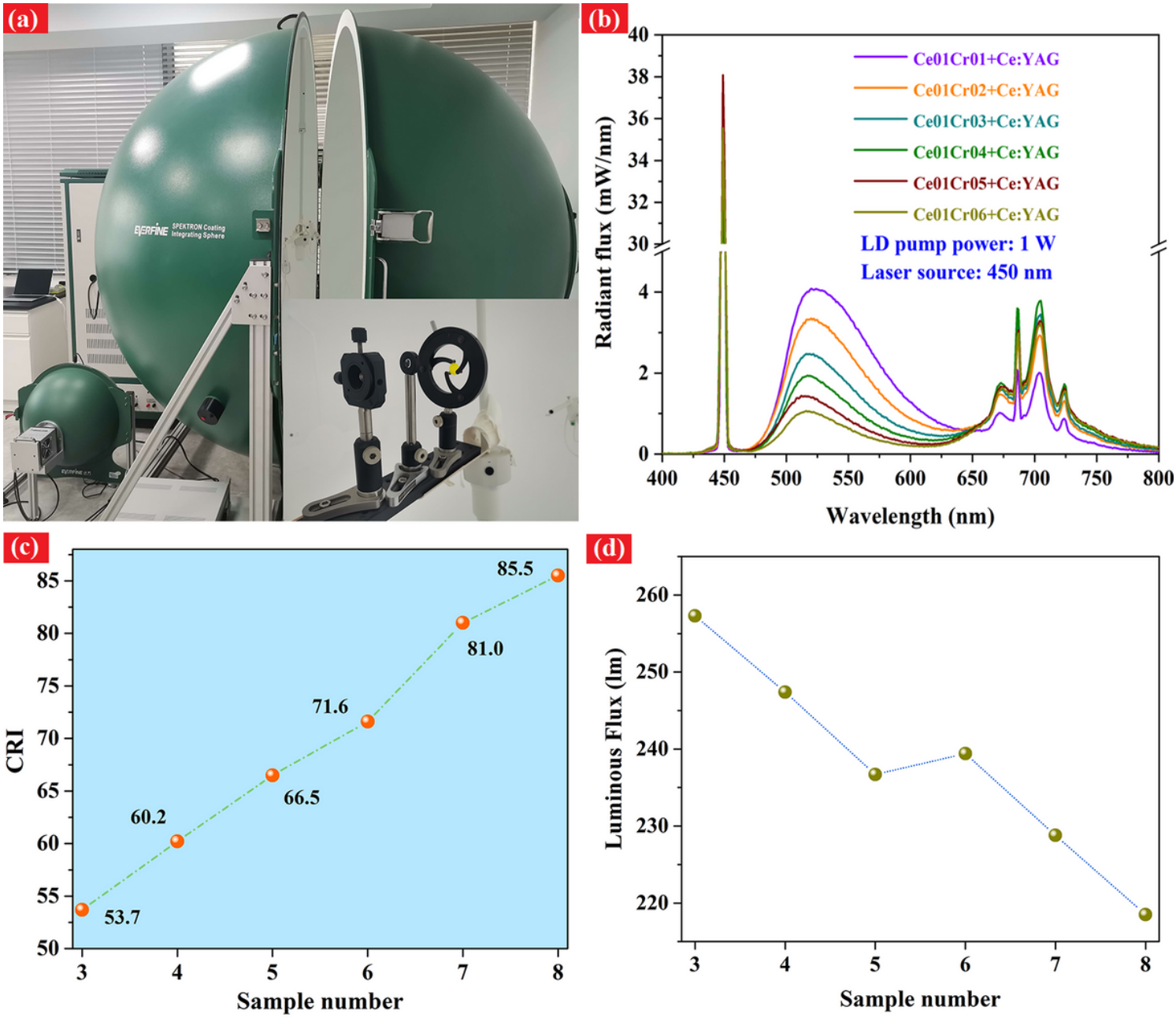

Figure 9

(a) Appearance of the apparatus for the LD measurement, (b) EL spectra, (c) CRI values and (d) luminous flux of the combined Ce,Cr:LuAG/Ce:YAG TC based LDs under 455 nm excitation.

Supplementary Files

This is a list of supplementary files associated with this preprint. Click to download.

- SupplementaryMaterial.doc